3.2 SPECIFIC DEVICES

Let us now focus on several selected silicon photonic devices and understand their operation principles with more details.

3.2.1 Modulator Based on Carrier Depletion in Silicon

In Ref. [16] the authors presented the realization of a high-speed silicon modulator based on carrier depletion in silicon waveguide. The basic phenomenon is related to the plasma dispersion effect mentioned in the previous chapter of this book. The free carriers' generation is related to depletion region of pn junctions. The device described in Ref. [16] is based on an MZI with a reverse-biased pn diode embedded in each of the two arms of the interferometer. The MMI coupler is used because it has a broader range of operating wavelengths and larger fabrication tolerance as compared to a directional coupler.

The fabrication process was designed to target the pn junction at approximately 0.4 μm above the buried oxide to enable optimal modal overlap with the depletion region. As the n-doping concentration is much higher than the p-doping concentration, carrier depletion under reverse bias occurs mainly in the p-type doped region which results by improved phase modulation efficiency due to the hole density change providing larger refractive index change as compared to the electron density change.

Note that pn junction-based silicon modulator has a fast intrinsic response (the transverse response time is ~7 ps). However, in order to obtain the high-frequency operation it is essential to overcome the issues associated with the relatively large pn junction capacitance and metal contact parasitics. To minimize the *RC* limitation of the frequency response of the modulator the authors of Ref. [16] realized traveling wave electrode based on coplanar waveguide structure. The RF traveling wave coplanar waveguide and modulator optical waveguide are carefully designed so that both electrical and optical signals co-propagate along the length of the phase shifter with similar speeds, while, at the same time, the RF attenuation is kept as small as possible.

For a reverse-biased pn junction, the depletion width depends on the bias voltage and doping concentrations. For the asymmetrically doped pn junction as done in Ref. [16] the depletion width (W_D) can be approximated following the formulations presented in the theoretical background chapter on semiconductors:

$$W_D = \sqrt{\frac{2\varepsilon_0\varepsilon_r\left(V_{bi} + V_{in}\right)}{qN_A}} \tag{3.2}$$

where ε_0 and ε_r are the vacuum permittivity and the low-frequency relative permittivity of silicon, q is the electron charge, N_A is the acceptor concentration, V_{bi} is the built-in voltage and V_{in} is the applied voltage. Changing the depletion width of a pn junction is equivalent to changing the free carrier density. Thus, by changing the bias voltage, one can achieve refractive index modulation through the free carrier plasma dispersion effect.

Photonic modulators based upon the depletion region have small signal transient response which determines the feasibility of the device to be used for high-speed data modulation. The small signal response will be defined by the depletion or junction capacitance C_J [15]. Following the technical

background given in the chapter on semiconductors, the capacitance associated with the depletion region C_J is given by:

$$C_J = A\sqrt{\frac{q\varepsilon_s N_A N_D}{2(N_A + N_D)\cdot(\psi_B + V_D)}}$$

where A is the area of the junction, q is the charge of an electron, ε_S is the permittivity of silicon, N_A is the concentration of acceptors, N_D is the concentration of donors, ψ_B is the potential difference at the junction and V_D is the voltage applied to the junction.

3.2.2 Modulators Based on Resonators

3.2.2.1 Background on Integrated Resonators

Due to the fact that the electro-photonic interaction of light and matter in silicon has relatively small coefficients, in order to be able to realize photonic devices with reduced interaction length many silicon photonic devices are based upon resonators, e.g. ring resonators. Micro-ring resonators are versatile wavelength-selective elements that can be used to synthesize a wide class of filter functions [63,64]. Many theoretical designs have been proposed to optimize the filter response and other properties using various coupled resonator arrays [65,66], while compact resonators have been demonstrated in a number of semiconductor materials [67] and glass waveguides [68]. The finesse of the resonator is related to the number of times that the light travels through the resonator (e.g. a ring) and thus if high finesse is realized, more compact devices can be used.

The operation principle of ring resonators is similar to the basic concept of the Fabry–Perot resonator. Let us assume the schematic sketch shown in Figure 3.10.

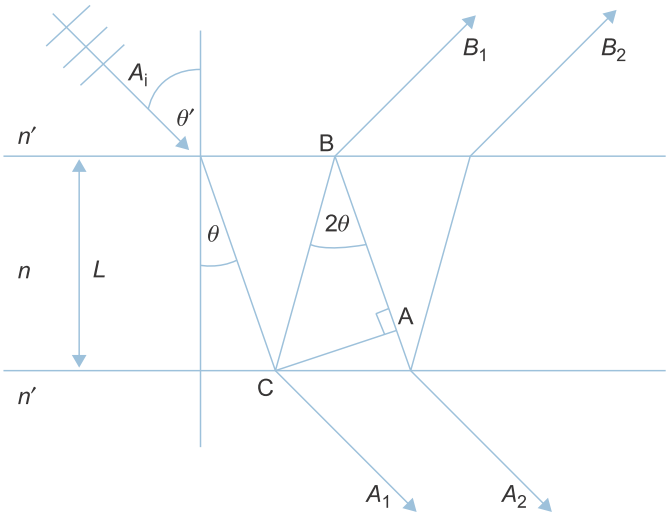

FIGURE 3.10

Schematic sketch of rays reflected between two mirrors separated by a distance L.

The refractive index of the material between two mirrors is denoted by n and the refractive index of the materials outside the mirrors by n'. We assume that an incident ray with an amplitude of A_i is arriving at the first mirror surface at an angle of θ'. The amplitudes of the back-reflected beams are B_1, B_2 etc., while the subscript indicates the order of reflection. The amplitudes of the transmitted beams are denoted by A_1, A_2 etc., while again the subscript indicates the order of transmission. We assume that the transmission coefficient for the electrical field when going from material n' towards material n is denoted by t and the transmission coefficient for light going in the opposite direction is t'. The reflective coefficients for the field are denoted as Γ and Γ'' for beam that is back-reflected from material with refraction index of n or n' respectively.

Let us start by computing the length of the paths CB and BA which are responsible for the phase optical path difference generated between any two adjacent transmitted beams. The sum of the paths equals:

$$CB + BA = 2L\cos\theta \tag{3.3}$$

Thus the optical path difference will be:

$$\delta = \frac{2\pi n}{\lambda_V}(CB + BA) = \frac{4\pi nL}{\lambda_V}\cos\theta = \frac{4\pi n\nu}{c}\cos\theta \tag{3.4}$$

where λ_V is the wavelength in vacuum and c is the speed of light in vacuum. The coefficients of the reflected field are:

$$\begin{aligned} B_1 &= \Gamma A_i \\ B_2 &= tt'\Gamma' A_i \exp(i\delta) \\ B_3 &= tt'\Gamma' A_i \exp(i\delta)\left(\Gamma'^2 \exp(i\delta)\right) \\ &\vdots \\ B_n &= B_{n-1}\left(\Gamma'^2 \exp(i\delta)\right) \end{aligned} \tag{3.5}$$

Using the geometrical series expression yields:

$$B_{tot} = \sum_n B_n = A_i\left(\Gamma + tt'\Gamma'\frac{\exp(i\delta)}{1 - \Gamma'^2\exp(i\delta)}\right) \tag{3.6}$$

The expressions for the amplitudes of the transmitted field yield:

$$\begin{aligned} A_1 &= A_i tt' \exp(i\delta') \\ A_2 &= A_i tt' \exp(i\delta')\left(\Gamma'^2 \exp(i\delta)\right) \\ A_3 &= A_i tt' \exp(i\delta')\left(\Gamma'^2 \exp(i\delta)\right)^2 \\ &\vdots \\ A_n &= A_{n-1}\left(\Gamma'^2 \exp(i\delta)\right) \end{aligned} \tag{3.7}$$

and the final results of the summation equal:

$$A_{tot} = \sum_n A_n = A_i tt'\Gamma' \frac{\exp(i\delta')}{1-\Gamma'^2\exp(i\delta)} \tag{3.8}$$

where

$$\delta' = \frac{2\pi n}{\lambda_V}\frac{L}{\cos\theta} \tag{3.9}$$

Following the Stokes principle we have:

$$\begin{aligned} \Gamma' &= -\Gamma \\ tt' &= 1-\Gamma^2 \end{aligned} \tag{3.10}$$

Thus, one may obtain that the reflection or transmitted ratios equal:

$$\begin{aligned} \frac{A_{tot}}{A_i} &= \left(1-\Gamma^2\right)\frac{\exp(i\delta')}{1-\Gamma^2\exp(i\delta)} \\ \frac{B_{tot}}{A_i} &= \Gamma\frac{1-\exp(i\delta)}{1-\Gamma^2\exp(i\delta)} \end{aligned} \tag{3.11}$$

Those relations are for the electric field. For intensities one obtains:

$$\begin{aligned} \frac{I_t}{I_i} &= \frac{|A_{tot}|^2}{|A_i|^2} = \frac{(1-R)^2}{(1-R)^2 + 4R\sin^2(\delta/2)} \\ \frac{I_r}{I_i} &= \frac{|B_{tot}|^2}{|A_i|^2} = \frac{4R\sin^2(\delta/2)}{(1-R)^2 + 4R\sin^2(\delta/2)} \end{aligned} \tag{3.12}$$

where R is the reflection coefficient for the intensity:

$$R = |\Gamma|^2 \tag{3.13}$$

One may clearly see the conservation of energy, since:

$$\frac{I_r}{I_i} + \frac{I_t}{I_i} = 1 \tag{3.14}$$

Optical frequencies of maximal transmission are obtained when the expression for I_t/I_i is maximized, i.e. for:

$$\nu_m = m\frac{c}{2nL\cos\theta} \tag{3.15}$$

where m is an integer number. The distance between two transmission peaks, also called the free spectral range (FSR), is equal to:

$$\Delta\nu = \nu_{m+1} - \nu_m = \frac{c}{2nL\cos\theta} \tag{3.16}$$

and in order to convert this equation to wavelength units, we use the well-known relation of:

$$\lambda_m \nu_m = c, \tag{3.17}$$

to obtain:

$$\Delta\lambda = \frac{c}{\nu^2}\Delta\nu = \frac{\lambda^2}{c}\Delta\nu \tag{3.18}$$

yielding:

$$\Delta\lambda = \frac{\lambda^2}{2nL\cos\theta} \tag{3.19}$$

From Eq. 3.16 one may extract the frequencies of the peaks:

$$\nu_m = m\Delta\nu \tag{3.20}$$

Defining the criteria of half width half maximum (HWHM) as the width of each transmission peak:

$$I_t = \frac{I_i}{2} \tag{3.21}$$

yields the following:

$$4R\sin^2\left(\delta_{1/2}/2\right) = \left(1-R\right)^2 \tag{3.22}$$

which results in:

$$\text{HWHM} = \delta_{1/2} - 2m\pi = \frac{1-R}{\sqrt{R}} \tag{3.23}$$

Thus, the width of the peak is equal to:

$$\Delta\nu_{1/2} = \frac{c}{4\pi nL\cos\theta}\cdot\delta = \frac{c}{4\pi nL\cos\theta}\cdot 2\left(\delta_{1/2} - 2m\pi\right) \tag{3.24}$$

or:

$$\Delta\nu_{1/2} = \frac{c}{2\pi nL\cos\theta}\cdot\frac{1-R}{\sqrt{R}} = \frac{\Delta\nu}{\pi}\cdot\frac{1-R}{\sqrt{R}} \tag{3.25}$$

Following that, the finesse of the resonator is defined as:

$$\Im = \frac{\Delta\nu}{\Delta\nu_{1/2}} = \pi\frac{\sqrt{R}}{1-R} \tag{3.26}$$

The main advantage of using a ring resonator is the good match it proposes for integrated circuits and waveguides. The theory of ring resonators is similar to the previously developed insights on Fabry–Perot. However, some parameters are expressed differently. Ring resonators sometimes have four terminals coupled together through two couplers. The coupling efficiency is determined according to the proximity between the waveguides and the ring structure in the center of the resonator (schematic sketch is seen in Fig. 3.11).

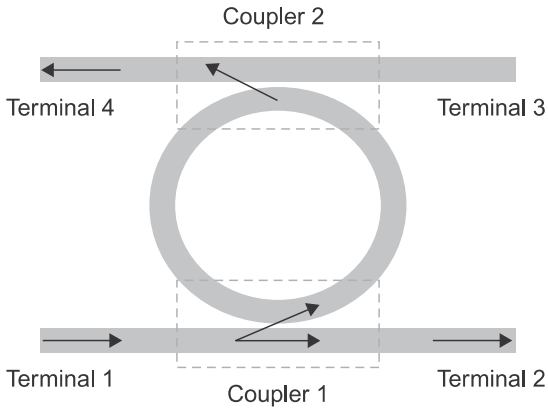

FIGURE 3.11

Schematic sketch of ring resonator.

If a wavelength λ_m satisfies the resonant condition of

$$n_{eff}\pi D = m\lambda_m \tag{3.27}$$

and is input through terminal 1, the coupling of the wave with that wavelength will be enhanced and all others will be suppressed. As a result, only this wavelength will be dropped from terminal 4, while the rest of the wavelengths will pass through and output from terminal 2. In the last equation n_{eff} is the effective refractive index of the bending waveguide, D is the diameter of the ring and m is an integer. If observing again Eq. 3.15 and using the relation connecting the optical wavelength and the optical frequency (Eq. 3.17) one obtains that for Fabry–Perot the resonance condition is:

$$n_{eff}\,2L\cos\theta = m\lambda_m \tag{3.28}$$

and thus by choosing πD$\sim 2L\cos\theta$ both equations will coincide, simply because πD represents the circumference of the ring. The FSR is one of the key specifications of the ring resonator. It is defined as:

$$\text{FSR} = \frac{\lambda_m^{\,2}}{n_{eff}\left(\pi D + L_c\right)} \tag{3.29}$$

where L_c is the length of the coupler. If comparing this with Eq. 3.19 one may see that for $\pi D + L_c \sim 2L\cos\theta$ both equations coincide.

Because the FSR is inversely proportional to the size of the ring resonator, the ring must be small in order to achieve a high FSR. The finesse of the ring resonator is defined in the same way as in Fabry–Perot (Eq. 3.26) but the "reflectivity" R is defined as:

$$R = \exp(-\alpha)(1-\kappa) \tag{3.30}$$

where α is the total amplitude attenuation coefficient for each round trip, and κ is the normalized coupling coefficient of the coupler.

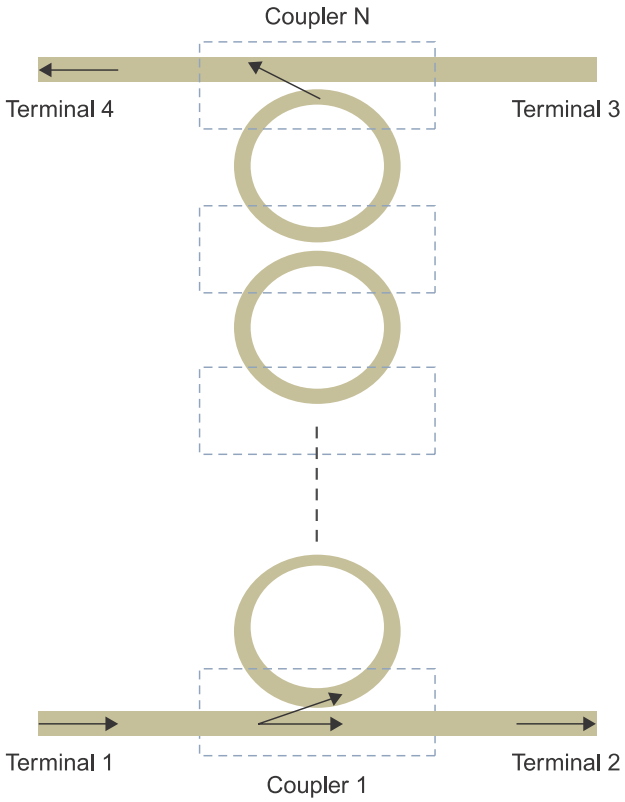

FIGURE 3.12

Schematic sketch of multiple ring resonators.

It is almost always advantageous to reduce both the internal and external losses in order to obtain higher finesse. However, the external loss due to coupling is necessary and cannot be too small for the resonator to operate as an optical filter. If the external loss is smaller than the internal loss, all the coupled power will be lost inside the cavity and no power will be coupled out. Because of these constraints, the ring resonator must use a strongly guided waveguide to minimize the bending loss for a curved waveguide with a very small radius.

One option to increase the finesse is to use multiple ring resonators where two or more rings could be coupled in cascade as shown in Figure 3.12. In this case, the FSR is increased and the combined FWHM is accordingly reduced. The various resonators have to be carefully designed to make sure that the spectral position of the desired resonance wavelength will coincide in all of the cascaded resonators.

An important parameter is the quality factor Q which is directly proportional to the finesse as follows:

$$Q = \frac{n_{eff}\pi D}{\lambda_m}\Im \tag{3.31}$$

3.2.2.2 Resonator Based on Low Refractive Index Holes

The device described in Ref. [27] includes a Fabry–Perot resonator that is realized by creating low-refractive-index holes in silicon waveguide in order to realize reflective mirrors. It is well known that the Fresnel reflection coefficients, generated when an optical beam passes between two mediums with different refraction index, are equal to:

$$R = \left(\frac{n_1 - n_2}{n_1 + n_2}\right)^2 \tag{3.32}$$

where n_1 and n_2 are the refraction indices of the two mediums. In the case described in Ref. [27] and in Figure 3.9, air holes are generated in the silicon waveguide. Since the refraction index of silicon is about $n_1 = 3.5$ and if air holes are created then $n_2 = 1$ and we have $R = 0.3$. If the periodic structure

of such holes is realized a Bragg mirror can be generated for wavelength corresponding to twice the distance between adjacent holes (denoted by Λ) multiplied by the effective refraction index n_{eff}:

$$\lambda_m = 2\Lambda n_{eff} \tag{3.33}$$

If this wavelength corresponds with the resonance condition of Fabry–Perot (see Eq. 3.28) then a matched resonator is realized. The refraction index of the cavity is modified due to the plasma dispersion effect leading to realization of a modulation depth (*MD*) of:

$$MD \propto \frac{\delta\lambda_{Resonance\,Shift}}{\Delta\lambda_{HWHM}} \tag{3.34}$$

where $\delta\lambda_{Resonance\ Shift}$ is the absolute shift of the resonance peak, $\Delta\lambda_{FWHM}$ is the full-width half maximum of the resonance, which is a measure of the bandwidth of the device, and Q is the quality factor (see Eqs. 3.25 and 3.31). The shift of the resonance $\delta\lambda_{Resonance\ Shift}$ is directly proportional to the change in the refraction index (see Eqs. 3.15 and 3.17).

The change in the refraction index is proportional to P, being the power required to maintain a certain number of steady-state absolute carriers in a given geometry, divided by the length L of the device at a certain carrier concentration for a given cross-sectional area A. This is because the concentration of the generated free carriers is proportional to the absorbed power per relevant unit of volume. This concentration eventually changes the refraction index of the resonator following the well-known plasma dispersion effect that was previously explained. Therefore one may write:

$$MD \propto \frac{Q \cdot P}{A \cdot L}$$

A figure of merit (FOM) for these modulators is the total amount of bandwidth desired at a certain modulation depth, and the power required to do so. Using Eq. 3.34 one obtains that:

$$\text{FOM} = \frac{MD \cdot Bandwidth}{P} \propto \frac{1}{V_{eff}} \tag{3.35}$$

where $V_{eff} = AL$ is the effective volume of the refractive index-changing cavity region.

In the configuration as proposed by Ref. [27] where the authors use linear Fabry–Perot cavity with a cavity length of only 2.51 μm one may obtain V_{eff} as small as $3.4(\lambda/n_{eff})^3$. This is a very small number defining a large FOM. A ring resonator with diameter of 10 μm has V_{eff} that is more than 12 times larger.

3.2.2.3 Carrier-Injected Micro Ring Resonator-Based Modulator

In Ref. [20] a micro ring resonator is used where the modulation is obtained using carrier injection which modifies the refraction index of the resonator due to the plasma dispersion effect. The operation speed of the p-i-n modulator is conventionally thought to be limited by the relatively slow carrier dynamics in the junction. However, the optical response time, in contrast to the electrical response time, can be much shorter thanks to the non-linear transfer function of the device, enabling much

faster modulation. The non-linear relationship between the optical transmission T at wavelength of λ_0 and the total charge q_{tot} in the junction is given by [20]:

$$T = \frac{\left(\frac{2q_{tot}\Gamma_0\gamma Q}{qn_gV_{eff}}\right)^2}{1+\left(\frac{2q_{tot}\Gamma_0\gamma Q}{qn_gV_{eff}}\right)^2} \tag{3.36}$$

where q is the charge of an electron, $n_g = 4.3$ is the group index of the ring, $V_{eff} = 4.5 \times 10^{-12}[\text{cm}^3]$ is the volume of the junction, $\Gamma_0 = 0.8$ is the mode confinement factor, $\gamma \approx 4.3 \times 10^{-21}[\text{cm}^3]$ is the ratio between the change of refractive index of silicon and the electron-hole-pair density ΔN when $\Delta N \approx 10^{17}[\text{cm}^{-3}]$ and $Q \approx 20\,000$ is the quality factor of the ring resonator.

For simplicity, we assume that the ring resonator is critically coupled to the waveguide, so that the optical transmission is zero at λ_0. When the p-i-n diode is forward biased, the electron and hole densities in the intrinsic region are equal, which means that the total charge carried by electrons and holes satisfies $-q_e = q_h = q_{tot}$. Under dynamic driving voltage, the charge q_{tot} in the junction follows the first-order differential equation involving the serial resistance of the diode and the average carrier recombination lifetime in the device (denoted as τ). The rise time of the optical transmission is much shorter than the rise time of the charge dynamics, which is determined by the carrier dynamics with positive bias voltage.

The rise time of the charge injection, defined as the time needed for q_{tot} to reach 0.9 of the steady-state charge, is proportional to τ. On the other hand one can see that the optical transmission quickly saturates to about 100% as the charge q_{tot} increases. Specifically, the transmission $T > 90\%$ as long as we have charge of $q_{tot} > 3qn_gV_{eff}/2q_{tot}\Gamma_0\gamma$. Therefore, the optical rise time is only determined by the time needed to inject this amount of charge into the junction, which can be much shorter than the rise time of charge injection, if this charge is smaller than the steady-state charge.

Note that the photon lifetime of a ring resonator at λ_0 resonance can be obtained from the quality factor as:

$$\tau_{cav} = \frac{Q\lambda_0}{2\pi c} \tag{3.37}$$

where c is the speed of light. This lifetime can be equal to 9.1 ps in case of a ring resonator with Q factor of about 10 000 (and a diameter of 10 μm as presented in Ref. [38]) and at wavelength around 1550 nm. This lifetime gives the fundamental limit to the operation speed of the device which once again can be a very high one and to match the constantly increasing requirements in the field of optics communication.

References

[1] R.A. Soref, B.R. Bennett, Electro-optical effects in silicon, IEEE J. Quantum Electron. 23 (1987) 123–129.
[2] S.T. Feng, E.A. Irene, Thermo-optical switching in Si based etalons, J. Appl. Phys. 72 (1992) 3897–3903.
[3] R.L. Espinola, M.C. Tsai, J.T. Yardley, R.M. Osgood, Fast and low-power thermo-optic switch on thin silicon-on-insulator, IEEE Photon. Technol. Lett. 15 (2003) 1366–1368.

[4] L. Pavesi, D.J. Lockwood, Silicon Photonics, in vol. 94, Topics in Applied Physics Series, Springer, New York, 2004.
[5] G.T. Reed, A.P. Knights, Silicon Photonics: An Introduction, Wiley, Chichester, UK, 2004.
[6] R.S. Jacobsen, K. Andersen, P.I. Borel, J. Fage-Pedersen, L.H. Frandsen, O. Hansen, et al., Strained silicon as a new electro-optics material, Nature 441 (2006) 199–202.
[7] G.T. Reed, The optical age of silicon, Nature 427 (2004) 595–596.
[8] A. Liu, R. Jones, L. Liao, D. Samara-Rubio, D. Rubin, O. Cohen, et al., A high speed silicon optical modulator based on a metal-oxide-semiconductor capacitor, Nature 427 (2004) 615–618.
[9] L. Liao, D. Samara-Rubio, M. Morse, A. Liu, D. Hodge, D. Rubin, et al., High speed silicon Mach–Zehnder modulator, Opt. Exp. 13 (2005) 3129–3135.
[10] A. Liu, D. Samara-Rubio, L. Liao, M. Paniccia, Scaling the modulation bandwidth and phase efficiency of a silicon optical modulator, IEEE J. Sel. Top. Quantum Electron. 11 (2005) 367–372.
[11] D. Samar-Rubio, U.D. Keil, L. Liao, T. Franck, A. Liu, D.W. Hodge, et al., Customized drive electronics to extended silicon optical modulators to 4Gb/s, J. Lightwave Technol. 23 (2005) 4305–4314.
[12] G.V. Treyz, P.G. May, J.M. Halbout, Silicon Mach–Zehnder waveguide interferometers based on the plasma effect, Appl. Phys. Lett. 59 (1991) 771–773.
[13] C.K. Tang, G.T. Ree, Highly efficient optical phase modulator in SOI waveguides, Electron. Lett. 31 (1995) 451–452.
[14] P. Dainesi, A. Kung, M. Chabloz, A. Lagos, P. Fluckiger, A. Ionescu, et al., CMOS compatible fully integrated Mach–Zehnder interferometer in SOI technology, IEEE Photon. Technol. Lett. 12 (2000) 660–662.
[15] F. Gardes, G. Reed, N. Emerson, C. Png, A sub-micron depletion-type photonic modulator in silicon-on-insulator, Opt. Exp. 13 (2005) 8845–8854.
[16] A. Liu, L. Liao, D. Rubin, H. Nguyen, B. Ciftcioglu, Y. Chetrit, et al., High-speed optical modulation based on carrier depletion in a silicon waveguide, Opt. Exp. 15 (2) (2007) 660–668.
[17] J.M. Choi, R.K. Lee, A. Yariv, Control of critical coupling in a ring resonator fiber configuration: application to wavelength-selective switching, modulation, amplification, and oscillation, Opt. Lett. 26 (2001) 1236–1238.
[18] R.D. Kekatpure, M.L. Brongersma, R.S. Shenoy, Design of a silicon-based field-effect electro-optic modulator with enhanced light-charge interaction, Opt. Lett. 30 (2005) 2149–2151.
[19] C. Li, L. Zhou, A.W. Poon, Silicon micro-ring carrier-injection-based modulators/switches with tunable extinction ratios and OR-logic switching by using waveguide cross-coupling, Opt. Exp. 15 (2007) 5069–5076.
[20] Q. Xu, S. Manipatruni, B. Schmidt, J. Shakya, M. Lipson, 12.5 Gbit/s carrier-injection-based silicon micro-ring silicon modulators, Opt. Exp. 15 (2007) 430–436.
[21] Q. Xu, B. Schmidt, S. Pradhan, M. Lipson, Micrometre-scale silicon electro-optic modulator, Nature 435 (2005) 325–327.
[22] Q. Xu, B. Schmidt, J. Shakya, M. Lipson, Cascaded silicon micro-ring modulators for WDM optical interconnection, Opt. Exp. 14 (2006) 9431–9435.
[23] G. Shabtay, E. Eidinger, Z. Zalevsky, D. Mendlovic, E. Marom, Tunable birefringent filters – optimal iterative design, Opt. Exp. 10 (2002) 1534–1541.
[24] Z. Zalevsky, F. Luan, W.J. Wadsworth, S.L. Saval, T.A. Birks, Liquid crystal based in-fiber tunable spectral structures, Opt. Eng. 45 (2006) 335005.
[25] I. Abdulhalim, Unique optical properties of anisotropic helical structures in a Fabry–Perot cavity, Opt. Lett. 31 (2006) 3019–3021.
[26] C.A. Barrios, V.R. Almeida, R.R. Panepucci, B.S. Schmidt, M. Lipson, Compact silicon tunable Fabry–Perot resonator with low power consumption, IEEE Photon. Technol. Lett. 16 (2004) 506–508.
[27] B. Schmidt, Q. Xu, J. Shakya, S. Manipatruni, M. Lipson, Compact electro-optic modulator on silicon-on-insulator substrates using cavities with ultra-small modal volumes, Opt. Exp. 15 (2007) 3140–3148.

[28] J. Scheuer, A. Yariv, Two-dimensional optical ring resonators based on radial Bragg resonance, Opt. Lett. 28 (2003) 1528–1530.
[29] A. Liu, H. Rong, R. Jones, O. Cohen, D. Hak, M. Paniccia, Optical amplification and lasing by stimulated Raman scattering in silicon waveguides, J. Lightwave Technol. 24 (2006) 1440–1455.
[30] H. Rong, A. Liu, R. Jones, O. Cohen, D. Hak, R. Nicolaescu, et al., An all-silicon Raman laser, Nature 433 (2005) 292–294.
[31] H. Rong, R. Jones, A. Liu, O. Cohen, D. Hak, A. Fang, et al., A continuous wave Raman silicon laser, Nature 433 (2005) 725–728.
[32] R. Claps, D. Dimitropoulos, V. Raghunathan, Y. Han, B. Jalali, Observation of stimulated Raman amplification in silicon waveguides, Opt. Exp. 11 (2003) 1731–1739.
[33] R. Claps, V. Raghunathan, D. Dimitropoulos, B. Jalali, Anti-Stokes Raman conversion in silicon waveguides, Opt. Exp. 11 (2003) 2862–2872.
[34] O. Boyraz, B. Jalali, Demonstration of a silicon Raman laser, Opt. Exp. 12 (2004) 5269–5273.
[35] M.A. Foster, A.C. Turner, J.E. Sharping, B.S. Schmidt, M. Lipson, A.L. Gaeta, Broad-band optical parametric gain on a silicon photonic chip, Nature 441 (2006) 960–962.
[36] S. Fathpour, B. Jalali, Energy harvesting in silicon optical modulators, Opt. Exp. 14 (2006) 10795–10799.
[37] K.K. Tsia, S. Fathpour, B. Jalali, Energy harvesting in silicon wavelength converters, Opt. Exp. 14 (2006) 12327–12333.
[38] Q. Xu, M. Lipson, All-optical logic based on silicon micro-ring resonators, Opt. Exp. 15 (2007) 924–929.
[39] J. Liu, D. Pan, S. Jongthammanurak, K. Wada, L.C. Kimerling, J. Michel, Design of monolithically integrated GeSi electro-absorption modulators and photodetectors on a SOI platform, Opt. Exp. 15 (2007) 623–628.
[40] O.I. Dosunmu, D.D. Cannon, M.K. Emsley, L.C. Kimerling, M.S. Unlu, High-speed resonant cavity enhanced Ge photodetectors on reflecting Si substrates for 1550-nm operation, IEEE Photon. Technol. Lett. 17 (2005) 175–177.
[41] S.J. Koester, G. Dehlinger, J.D. Schaub, J.O. Chu, Q.C. Ouyang, A. Grill. Germanium-on-insulator photodetectors. In: 2nd IEEE International Conference Group IV Photonics (2005) 171–173.
[42] M. Oehme, J. Werner, E. Kasper, M. Jutzi, M. Berroth, High bandwidth Ge p-i-n photodetector integrated on Si, Appl. Phys. Lett. 89 (2006) 071117.
[43] P. Bhattacharya, J. Sabarinathan, J. Topolaposancik, S. Chakravarty, P.-C. Yu, W. Zhou, Quantum dot photonic crystal light sources, Proc. IEEE 93 (2005) 1825–1838.
[44] M.B. Fischbein, M. Drndic, CdSe nanocrystal quantum-dot memory, Appl. Phys. Lett. 86 (2005) 193106.
[45] M.A Hines, P. Guyot-Sionnest, Synthesis and characterization of strongly luminescent ZnS-capped CdSe nanocrystals, J. Phys. Chem. 100 (1996) 468–471.
[46] B.O. Dabbousi, J. Rodriguez-Viejo, F.V. Mikulec, J.R. Heine, H. Mattoussi, R. Ober, et al., (CdSe)ZnS core-shell quantum dots: synthesis and characterization of a size series of highly luminescent nanocrystallites, J. Phys. Chem. B 101 (1997) 9463–9475.
[47] S. Coe, W.-K. Woo, M. Bawendi, V. Bulovic, Electroluminescence from single monolayers of nanocrystals in molecular organic devices, Nature 420 (2002) 800–803.
[48] S. Chaudhary, M. Ozkan, W.C.W. Chan, Trilayer hybrid polymer-quantum dot light-emitting diodes, Appl. Phys. Lett. 84 (2004) 2925–2927.
[49] S. Nizamoglu, T. Ozel, E. Sari, H.V. Demir, White light generation using CdSe/ZnS core-shell nanocrystals hybridized with InGaN/GaN light emitting diodes, Nanotech. 18 (2007) 065709.
[50] J. Liu, T. Tanaka, K. Sivula, A.P. Alivisatos, J.M.J. Fréchet, Employing end-functional polythiophene to control the morphology of nanocrystal–polymer composites in hybrid solar cells, J. Am. Chem. Soc. 126 (2004) 6550–6551.
[51] D. Qi, M.B. Fischbein, M. Drndic, S. Selmic, Efficient polymer–nanocrystal quantum-dot photodetectors, Appl. Phys. Lett. 86 (2005) 093103.

[52] E. Mutlugun, I.M. Soganci, H.V. Demir, Nanocrystal hybridized scintillators for enhanced detection and imaging on Si platforms in UV, Opt. Exp. 15 (2007) 1128–1134.
[53] Y. Okawachi, M. Foster, J. Sharping, A. Gaeta, Q. Xu, M. Lipson, All-optical slow-light on a photonic chip, Opt. Exp. 14 (2006) 2317–2322.
[54] H. Fukuda, K. Yamada, T. Shoji, M. Takahashi, T. Tsuchizawa, T. Watanabe, et al., Four-wave mixing in silicon wire waveguides, Opt. Exp. 13 (2005) 4629–4637.
[55] R. Espinola, J. Dadap, R. Osgood Jr., S. McNab, Y. Vlasov, C-band wavelength conversion in silicon photonic wire waveguides, Opt. Exp. 13 (2005) 4341–4349.
[56] H. Rong, Y.-H. Kuo, A. Liu, M. Paniccia, O. Cohen, High efficiency wavelength conversion of 10 Gb/s data in silicon waveguides, Opt. Exp. 14 (2006) 1182–1188.
[57] J. Sharping, Y. Okawachi, J. van Howe, C. Xu, Y. Wang, A. Willner, et al., All-optical, wavelength and bandwidth preserving, pulse delay based on parametric wavelength conversion and dispersion, Opt. Exp. 13 (2005) 7872–7877.
[58] Q. Lin, R. Jiang, C.F. Marki, C.J. McKinstrie, R. Jopson, J. Ford, et al., 40 GB/s optical switching and wavelength multicasting in a two-pump parametric device, IEEE Photon. Technol. Lett. 17 (2005) 2376–2378.
[59] E. Ciaramella, S. Trillo, All-optical reshaping via four-wave mixing in optical fibers, IEEE Photon. Technol. Lett. 12 (2000) 849–851.
[60] X. Li, P.L. Voss, J.E. Sharping, P. Kumar, Optical fiber source of polarization entangled photons in the 1550 nm telecom band, Phys. Rev. Lett. 94 (2005) 053601.
[61] Z. Zalevsky, A. Rudnitsky, M. Nathan, Nano photonic and ultra fast all-optical processing modules, Opt. Exp. 13 (2005) 10272–10284.
[62] A. Barkai, Y. Chetrit, O. Cohen, R. Cohen, N. Elek, E. Ginsburg, et al., Integrated silicon photonics for optical networks, J. Opt. Net. 6 (1) (2007) 25–47.
[63] M.K. Chin, S.T. Ho, Design and modeling of waveguide-coupled single-mode microring resonators, J. Lightwave Technol. 15 (1998) 1433–1446.
[64] B.E. Little, S.T. Chu, H.A. Haus, J. Foresi, J.-P Laine, Microring resonator channel dropping filters, J. Lightwave Technol. 15 (1997) 998–1005.
[65] G. Griffel, Synthesis of optical filters using ring resonator arrays, IEEE Photon. Technol. Lett. 12 (2000) 810–812.
[66] B.E. Little, S.T. Chu, W. Pan, Y. Kokubun, Microring resonator arrays for VLSI photonics, IEEE Photon. Technol. Lett. 12 (2000) 320–322.
[67] B.E. Little, J. Foresi, H.A. Haus, E.P. Ippen, W. Greene, S.T. Chu, Ultracompact Si/SiO_2 micro-ring resonator channel dropping filter, IEEE Photon. Technol. Lett. 10 (1998) 549–551.
[68] T. Kominato, Y. Ohmori, N. Takato, H. Okazaki, M. Yasu, Ring resonators composed of GeO_2-doped silica waveguides, IEEE J. Lightwave Tech. 10 (1992) 1781–1788.
[69] C.E. Png, G.T. Reed, R.M. Atta, G.J. Ensell, A.G.R. Evans, Development of small silicon modulators in silicon-on-insulator (SOI), Proc. SPIE 4997 (2003) 190–197 In: Photonics Packaging and Integration III, R. A. Heyler, D. J. Robbins, and G. E. Jabbour, (Eds).
[70] F. Gan, F.X. Kartner, High-speed silicon electrooptic modulator design, IEEE Photon. Technol. Lett. 17 (2005) 1007–1009.